8-10-2009

Mesoporosity and Functional Group Dependent Endocytosis and Cytotoxicity of Silica Nanomaterials

Zhimin Tao
Syracuse University

Bonnie B. Toms
Upstate Medical University, State University of New York

Jerry Goodisman
Syracuse University

Tewodros Asefa
Syracuse University

Mesoporosity and Functional Group Dependent Endocytosis and Cytotoxicity of Silica Nanomaterials

Zhimin Tao,[†,§] Bonnie B. Toms,[‡] Jerry Goodisman,[†] and Tewodros Asefa*[,†]

Department of Chemistry, Syracuse University, Center for Science and Technology, 1-014, Syracuse, New York 13244, and Department of Pediatrics, State University of New York, Upstate Medical University, 750 East Adams Street, Syracuse, New York 13210

Received August 10, 2009

We report different mesoporosity-dependent and functional group-dependent cytotoxicity and endocytosis of various silica nanomaterials on suspended and adherent cells. This dependency further varied with incubation time and particle dosage, and appeared to be associated with the particles' endocytotic efficiency and their chemical and physical properties. We studied two common mesoporous nanomaterials (MSNs), MCM-41 and SBA-15, and one type of solid-cored silica microsphere, paralleled by their quaternary amine functionalized counterparts. Compared to SBA-15, MCM-41 has a larger surface area but smaller pore size, whereas SMS exhibits low surface area and poor porosity. In Jurkat cells, SBA-15 and MCM-41 exhibited different cytotoxicity profiles. However, no significant cell death was detected when treated with the aminated MSNs, indicating that the positively charged quaternary amines prevented cellular injury from mesoporous nanoparticles. Furthermore, the effective internalization of MSN but not aminated-MSNs was clearly observed, in line with their consequent cytotoxicity. SK-N-SH (human neuroblastoma) cells were found to be more resistant to the treatment of MSN, whether aminated or not. Incubation with either SBA-15 or MCM-41 over time showed a recovery in cell viability, while exposure to MSN-N particles did not induce a noticeable cell death until longer incubation with high dosage of 200 μg/mL was applied. Both aminated and nonaminated silica spheres exhibited instant and constant toxicity on Jurkat (human T-cell lymphoma) cells. TEM images revealed successful endocytosis of SMS and SMS-N, although SMS-N appeared to accumulate more in the nucleus. For SK-N-SH cells, low dosage of SMS was found to be less toxic, whereas high dosage produced profound cell death.

1. Introduction

The introduction of nanotechnology into biology and medicine ushers the development of both material and biological sciences into a new era. Nanomaterials have been widely considered as promising candidates for drug delivery, gene transfection, medical imaging, and tumor targeting, mainly due to their highly ordered structure, unique physical and chemical properties, and large surface area (*1–12*). In particular, research breakthroughs on morphology control and surface functionalization have given the particles at nanometer scale a wide range of possible applications in biological systems (*13–19*). Consequently, the potential adverse effects of these particles on the environment or human health have attracted increasing attention from researchers, as reports on cytotoxicities of carbon nanotubes, quantum dots, or metal nanoparticles have mushroomed in the recent years (*20–27*). The possible cytotoxicities of nanomaterials could result from cellular injuries through a variety of mechanisms, such as membrane peroxidation, glutathione depletion, mitochondrial dysfunction, and DNA damage, eventually leading to cell death. Hence, systematic examinations concerning the biocompatibility of nanomaterials are necessary prior to their medicinal use.

Mesoporous silica nanoparticles (MSN) are synthesized by self-assembling the silica source (e.g., tetraethyl orthosilicate) with surfactant templates under conditions of various pH (*28–30*). The reactions lead to the formation of nanosized silica spheres or rods with different porous structures, distinguishable by characteristic mesostructures, pore size and volume, wall thickness, and surface area per unit mass. The large internal space of mesopores allows MSN to load biomolecules (such as hormones and proteins) or drugs and facilitates their delivery to intracellular destinations. This mini-Trojan Horse trespass can be further enhanced by grafting MSN with customized organic groups, either on the external surfaces or inside the mesoporous channels (*6–12*). The unique chemical and physical properties of MSN have been employed by researchers to fabricate efficient catalysts, sensitive biosensors, and site-directed drug carriers.

As elite members in the MSN family, MCM-41 and SBA-15 are currently examined as the next generation of drug delivery or neurotransmitter systems (*31–33*). Both types of MSN exhibited distinguishable differences in their individual lattice spacing, pore diameter, wall thickness, surface area, and shape regularity. Although the advantages of these MSNs for adsorption and release of pharmaceutical molecules have been widely studied, the cellular responses to treatment of these nanomaterials have been less examined. A few recent studies showed the rapid endocytosis of MCM-41 *in vitro* in various malignant or normal cell lines (*12, 34–37*). Further reports on cytotoxicity of silica nanoparticles suggested that low concentrations of MSN were more biocompatible than high doses (*38, 40*). Results from an *in vivo* mouse model treated by either MCM-41 or SBA-15 indicated that MSNs were non- or less-toxic to local tissues but induced serious systemic toxicity. Furthermore, it was

* Corresponding author. Tel: 1-315-443-3360. Fax: 1-315-443-4070. E-mail: tasefa@syr.edu.
[†] Syracuse University.
[‡] State University of New York.
[§] Present address: Department of Immunology and Genomic Medicine, Graduate School of Medicine, Kyoto University, Japan.

10.1021/tx900276u CCC: $40.75
Published on Web 10/09/2009

proposed that these toxicities could be lessened by decorating surfaces of the particles with certain functionalized groups (*40*), although this was not demonstrated experimentally. We previously studied the effects of MSN (SBA-15 and MCM-41) on cellular bioenergetics and showed that the mesoporous silicates impacted mitochondrial functions in a manner dependent on their physical properties (*38*). Both particles inhibited oxygen consumption by isolated mitochondria and submitochondrial particles, but only SBA-15 (not MCM-41) impaired cellular respiration in a dose-dependent manner (*38*). The submitochondrial particles (SMP), which are mitochondria with the inner membrane outside, were prepared by proper sonication (*41*). MSN particles at low concentrations (50 μg/mL) were found to have minimal effects on cellular ATP formation, while 200 μg/mL SBA-15 (not MCM-41) significantly diminished intracellular ATP formation. More interestingly, impairments by SBA-15 of either cell respiration or ATP synthesis changed over time, followed sometimes by a full recovery (*38*).

Here, we study the cellular uptake and cytotoxicity of MSNs. Comparison between MCM-41 and SBA-15 could point out the morphological effects on the different biological functions of these nanoparticles. To emphasize the effect of mesoporous structures on cellular responses, we utilized a silica microsphere (SMS, ~300 nm diameter) as a control in these experiments. Moreover, to examine the influence of functionalized groups, we also studied the endocytosis and cytotoxicity of organic grafted MSN and SMS with quaternary amines.

2. Experimental Section

2.1. Chemicals and Reagents. Cetyltrimethylammonium bromide (CTAB), tetraethyl orthosilicate (TEOS), and poly(ethylene oxide)-*block*-poly(butylene oxide)-*block*-poly(ethylene oxide) (P123, $EO_{20}PO_{70}EO_{20}$) were obtained from Sigma-Aldrich. *N*-Trimethoxysilylpropyl-*N*,*N*,*N*-trimethyl ammonium chloride ($C_9H_{24}ClNO_3Si$, abbreviated as TOSPTA, m.w. 257.83, 50% in methanol, and CAS# 35141-36-7) was purchased from Gelest, Inc. (Morrisville, PA).

2.2. Synthesis of SBA-15, MCM-41, and SMS Nanoparticles. SBA-15 was synthesized as reported by using P123 in acidic solution as a template (*28, 29*). Typically, a solution of $EO_{20}PO_{70}EO_{20}$/2 M HCl/tetraethoxysilane (TEOS)/H_2O = 2:60:4.25:15 (mass ratio) was stirred at 40 °C for 20 h and then aged at 80 °C for another 24 h. The solution was then filtered, and the solid was washed with a large amount of water resulting in as-synthesized SBA-15. This was followed by calcination of the as-synthesized sample to remove the template at 600 °C for 6 h with a heating ramp of 1 °C/min, followed by a cooling ramp of 2 °C/min.

The synthesis of MCM-41 was done by following a reported procedure with minor modification (*30, 31*). CTAB (4.0 g (1.1 mmol)) was dissolved in 960 mL of Millipore water and then mixed with 14 mL of 2.0 M NaOH solution. The solution was moderately stirred at 80 °C for 30 min, which was then followed by the addition of 22.6 mL (101.2 mmol) of TEOS. After stirring for another 2 h at 80 °C, the solution was filtered, and the precipitate was rinsed with Millipore water (4 × 80 mL), followed by rinsing with ethanol (4 × 80 mL) and drying in the oven at 80 °C. To remove the template, 6 g of the as-synthesized MCM-41 was stirred in a mixture of 3 mL (12.1 N) of hydrochloric acid and 600 mL of anhydrous ethanol at 50 °C for 5 h. The resulting material was filtered and washed with copious amounts of Millipore water and ethanol. The extracted MCM-41 was dried in the oven at 80 °C overnight before further modification of its surface.

Silica microspheres were synthesized by following a well-known Stöber method (*42–44*). TEOS (5.84 g) was added to 10 mL of 5 M ammonia solution (30 wt %) in a mixture of 50 mL of ethanol and 3.6 g of Millipore water under stirring to allow the hydrolysis of TEOS. After stirring for 12 h, a colloidal solution of silica spheres was obtained. The solution was centrifuged at 6500 rpm for 5 min, and the supernatant was decanted. The precipitate was then redispersed in a mixture of 20 mL of Millipore water and 20 mL of ethanol. The centrifugation and redispersing process was repeated several times to remove any unreacted chemicals. The resulting silica microspheres were dried before further modification.

2.3. Surface Functionalization of MSN and SMS with Quaternary Ammonium Groups. To functionalize all of the silica nanoparticles, 300 mg of the particles (SBA-15 after calcinations, MCM-41 after extraction, and SMS after synthesis) was dispersed in 150 mL of 2-propanol. Then, 1.15 mol (i.e., 615 μL) of *N*-trimethoxysilylpropyl-*N*,*N*,*N*-trimethyl ammonium chloride (TOSPTA, 50% in methanol) was added to the reaction mixture. The reaction was kept refluxing at 80 °C for 6 h, after which the solution was filtered, and the precipitate was rinsed with ethanol five times (80 mL each time). The final product was dried in the oven (overnight) before use. For simplicity, the amine-grafted samples were denoted as SBA-N, MCM-N, and SMS-N, respectively.

2.4. Characterizations of Silica Nanoparticles. The nitrogen physisorption measurement was carried out for all of the nanomaterials (with amine groups or without) at 77 K, using BET Micromertitics Tristar 3000 after outgassing the samples at 433 K for 2 h. This characterization also yielded total BET surface area, pore volume, and pore size distributions for each nanoparticle. Elemental analysis was later employed on amine-functionalized nanoparticles to measure the C, H, and N contents in all of the particles by weight.

2.5. Cell Cultures. The human T-cell lymphoma (Jurkat) and human neuroblastoma cells (SK-N-H) were obtained from the American Type Culture Collection (Manassas, VA). Jurkat cells were grown in standard RPMI 1640 media supplemented with 10% (v/v) fetal bovine serum with 100 μg/mL streptomycin, 100 IU penicillin, and 2.0 mM L-glutamine (Mediatech Inc., Herndon, VA). SK-N-H cells were cultured in EMEM (10−010) supplemented with 10% fetal bovine serum, 100 μg/mL streptomycin, 100 IU/mL penicillin, and 2.0 mM L-glutamine. Cell studies were carried out under standard conditions in a humidified, 37 °C, 5% CO_2 atmosphere. The neuroblastoma cells were removed from the flasks using a cell stripper (Mediatech, Herndon, VA) and counted using trypan blue (Mediatech, Herndon, VA). They were seeded in 75 cm^2 vented flasks, allowed to adhere overnight to the surface of the flask prior to the use for the incubations with nanoparticles. The average viability of each cell line was determined prior to seeding by light microscopy using a hemacytometer under standard trypan blue conditions.

2.6. Cytotoxicity Assay *in Vitro*. Cytotoxicities of MSN or SMS were evaluated on Jurkat and SK-N-SH cells by using the standard cell counting kit (CCK-8, Dojindo Molecular Technologies, Inc., Rockville, MD). A 96-well plate was utilized for the cell placement. Then, 100 μL/well cell-free media or cell suspension was distributed into a row of at least 6 wells for statistical purposes (n = 6−12). For SK-N-SH cells, 6000 cells per well were plated 24 h before the addition of nanoparticles. For Jurkat cells, 8000 cells/well were plated and immediately treated with nanoparticles. MSN, SMS, and the amine-grafted nanoparticles of three various concentrations (50, 100, and 200 μg/mL, respectively) were added. Plates were then incubated at 37 °C with 5% CO_2 for 3 days. Each day, the plates were taken, followed by the addition of 10 μL of WST-8 agent (i.e., 2-(2-methoxy-4-nitrophenyl)-3-(4-nitrophenyl)-5-(2,4-disulfophenyl)-2*H*-tetrazolium, monosodium salt), which can be bioreduced by cellular dehydrogenases to a water-soluble orange formazan product. The amount of this formazan product is proportional to the number of living cells. After another 3 h of incubation, the absorbance (Abs) was measured at 450 nm using a microplate reader. The result of subtracting the intensity of the cell-free medium with the addition of various nanoparticles from that of nanoparticle-treated cells gave an absorbance proportional to the number of living cells. The mitochondrial activity was hence measured quantitatively. The ratio between absorbance from cells treated with nanoparticles and that from untreated cells represents cell viabilities under various treatments (the viability of untreated cells was presumably 100%). Namely, cell viability was determined

as $\{(Abs_{treated} - Abs_{media}/Abs_{untreated} - Abs_{media}) \pm \text{standard deviation}\}$ % ($n = 6-12$).

2.7. Cell Images by TEM and Bright Field Microscopy. Jurkat cells (0.5 million cells/mL) were incubated with 200 μg/mL nanoparticles (SBA-5, MCM-41, and silica microsphere, grafted with or without quaternary amines) for 1 h and kept gently stirring. Then, 1.5 mL cell suspensions were collected and centrifuged. The cell pellets were soaked with 2.0% glutaraldehyde in 0.1 M cacodylate buffer (BOC, pH 7.4) for 2 h at 4 °C. The cell pellets were rinsed 3 times within the same BOC buffer, each time by 10 min of centrifugation. After careful washing, the cell pellets were mixed in BOC with 1% osmium tetroxide (OsO_4) for 1 h at 4 °C, followed by washing again 3 times with BOC. The resulting cell pellets were mixed with 2% agarose, forming jello-like cell samples. The cell samples were cut into pieces and subsequently dehydrated in 25% (10 min), 50% (10 min), 75% (overnight), 95% (10 min), 100% (10 min), and another 100% (10 min) ethanol. The polymerization process was completed by embedding cell samples in resin plates, infiltrated with a series of mixtures of resin and polyepoxide at ratios of 2:1 (4 h), 1:1 (4 h), and 1:2 (4 h), ending with 100% polyepoxide (4 h). The samples were then microtomed for TEM.

Bright field microscopy (Nikon EPIPHOTO 300, Japan) with built-in photographic equipment (Nikon FX-series) was utilized for observations of SK-N-SH cells under treatment of various nanoparticles. Cells were first replaced in a 96-well plate, and 24 h later, various concentrations of different nanoparticles were added. Then, 3 h after the addition of WST-8 reagent, the cells were taken for cell viability tests in a plate reader as well as for further morphological observations under bright filed microscopy.

3. Results and Discussion

3.1. Synthesis and Characterization of Nanoparticles. The syntheses of the MCM-41 and SBA-15 MSN were described in the Experimental Section. In the case of SBA-15, the synthesis was followed by calcination to remove the template; in the case of MCM-41, the as-synthesized sample was washed thoroughly in a mixture of HCl and ethanol. Both extraction processes result in the formation of orderly mesostructured nanoparticles. The transmission electron microscopy (TEM) images (Figure 1A and B) showed that the extracted MCM-41 nanomaterials were rather regular spherical particles of 300−350 nm in size, while the calcined SBA-15 materials were irregularly shaped particles of various sizes. These two kinds of MSNs were further characterized by nitrogen physisorption measurements, and both showed type IV isotherms with steep capillary condensation steps (Figures S1 and S2, Supporting Information), confirming the presence of mesoporous structures with large surface areas. For MCM-41, the BET surface area measurement gave a surface area of 1067 m^2/g. Porosity by the Barrett−Joyner−Halenda (BJH) method exhibited 31.5 Å averaged pore diameter and 1.08 cm^2/g cumulative pore volume. These results are summarized in Table 1. The SBA-15 nanomaterials have a measured surface area of 930 m^2/g, an averaged pore width of 59.2 Å, and a cumulative pore volume of 0.98 cm^3/g. Therefore, compared to SBA-15, MCM-41 owns a slightly bigger surface area and pore volume. However, the distinguishing difference of the MCM-41 material from its SBA-15 counterpart dwells in its much larger pore surface area (2.1-fold) but smaller pore size (0.5-fold). Spherical silica microspheres (SMS) were also synthesized by following the conventional Stöber method (*42–44*). Adjusting ammonia concentrations produced quite symmetrical silica spheres with a diameter of ~300 nm (Figure 1C). The nitrogen physisorption measurement of SMS gave a BET surface area of 11.3 m^2/g and a cumulative pore volume of 0.04 cm^3/g. The latter characteristics reflected a poor porosity of SMS nanoparticles, corroborating their solid-cored structure.

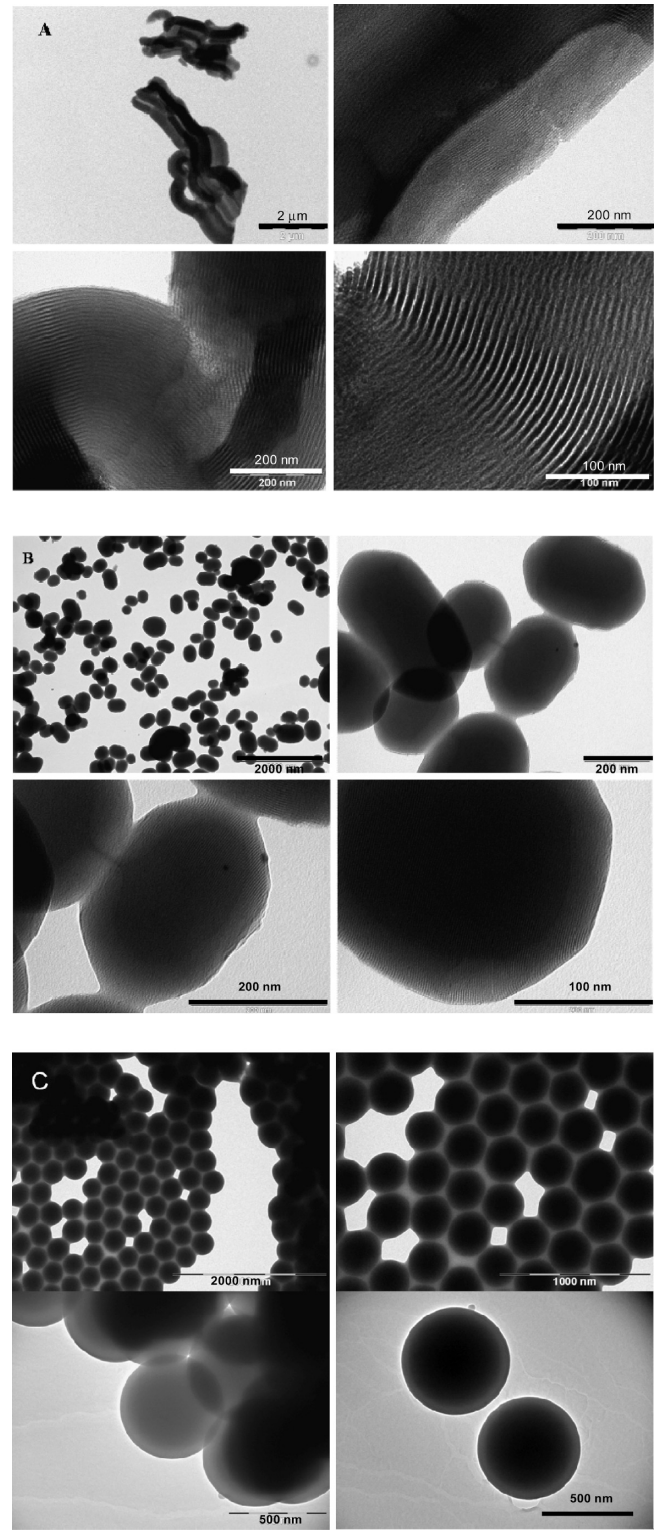

Figure 1. TEM images of (A) SBA-15, (B) MCM-41, and (C) SMS nanoparticles.

The surface functionalization of these nanoparticles was achieved by grafting amine groups, using *N*-trimethoxysilylpropyl-*N*,*N*,*N*-trimethylammonium chloride ($C_9H_{24}ClNO_3Si$, i.e., TOSPTA). As a result, the positively charged quaternary amines were tethered onto both external and internal surfaces of SBA-15 and MCM-41, and the external surface of SMS, to produce aminated particles (noted as SBA-N, MCM-N, and SMS-N, respectively). TEM images of all of these nanoparticles confirmed that their structures remained unchanged after amination (results not shown). Nevertheless, further nitrogen physisorption

Table 1. Characteristics of Silica Nanoparticles[a]

Type of nanoparticles	BET surface area (m^2/g)	BJH pore width (Å)	pore volume (cm^2/g)
MCM-41	1067	31.5	1.08
SBA-15	930	59.2	0.98
SMS	11	N/A	0.04
MCM-N	905	29.1	0.63
SBA-N	376	56.2	0.57
SMS-N	8	N/A	0.03

[a] BET surface area, average pore width, and pore volume are measured for ungrafted (MCM-41, SBA-15, and SMS) and grafted (MCM-N, SBA-N, and SMS-N) nanomaterials.

measurements revealed some changes in particle characters due to chemical grafting (see Table 1). For MCM-N, the nitrogen adsorption measurement gave a BET surface area of 905 m^2/g and a BJH pore diameter of 29.1 Å, slightly reduced from that of ungrafted MCM-41. In addition, the amine-functionalized MCM had a cumulative pore volume of 0.63 cm^3/g and pore surface area of 867 m^2/g (0.6- and 0.8-fold those of MCM-41, respectively), verifying the existence of the amine functional groups mostly inside the porous MCM channels. As for SBA-N, it showed a measured surface area of 376 m^2/g, an averaged pore width of 56.2 Å, and a cumulative pore volume of 0.57 cm^3/g. In contrast to those of SBA-15, the physical properties of functionalized samples were changed because of the reactions with quaternary amines. That is, the surface area of SBA-N became 0.4-fold smaller, and both the pore volume and surface area of SBA-15 became 0.4- and 0.6-fold smaller, implying that considerable amine groups were grafted on interior surfaces of SBA-N. For SMS-N particles, the gas physisorption measurement returned a surface area of 7.5 m^2/g (0.7-fold that of unaminated SMS) and a cumulative pore volume of 0.03 cm^3/g, showing the preservation of the solid structure of silica spheres with amine groups on the external surface of SMS-N.

All of the amine-functionalized silica nanoparticles were further characterized by elemental analyses (Table S1, Supporting Information). For MCM-N, the mass ratio among C, H, and N elements is 11.41:2.78:1.79; if converted to mole ratio, C:H:N = 8:22:1. This result was fairly consistent with the elemental composition of TOSPTA ($C_9H_{24}ClNO_3Si$), which confirms that the presence of C, H, and N elements in MCM-N is primarily due to the grafting of TOSPTA. Upon the basis of this fact, we calculated that 0.13 mol (i.e., 33.0 g) TOSPTA was grafted on every 100 g of MCM-N. For SBA-N nanomaterials, the mass ratio among C, H, and N elements is 9.45:2.32:1.36, i.e., C:H:N = 8:24:1 in mole ratio, which was quite in agreement with the elemental composition of TOSPTA, supporting the idea that the C, H, and N elements in SBA-N were principally introduced by TOSPTA amination. Hence, ~0.10 mol (i.e., 25.0 g) TOSPTA was grafted on every 100 g of SBA-N nanoparticles. For SMS-N particles, the composition of N elements was <0.05% by weight, suggesting an ineffective amination on the external surface of solid spheres. The mass ratio between C and H elements was 1.00:0.92, i.e., C:H = 1:11 in mole ratio. Therefore, relying on the component of C element in the samples, we calculated that <0.01 mol (i.e., 2.5 g) TOSPTA was grafted on every 100 g of SMS-N.

3.2. Cytotoxicity of Silica Nanoparticles. The quantitative measurements of the cytotoxicity of the nanomaterials were performed by following the procedures described in the Experimental Section. Figure 2A and Table 2 demonstrate the cell viability in the presence of different concentrations of SBA-15 nanoparticles. Apparently, at a low dosage of 50−100 μg/mL, SBA-15 nanomaterials had a minimal effect on the viability of Jurkat cells during a short time exposure of 3 h. However, at

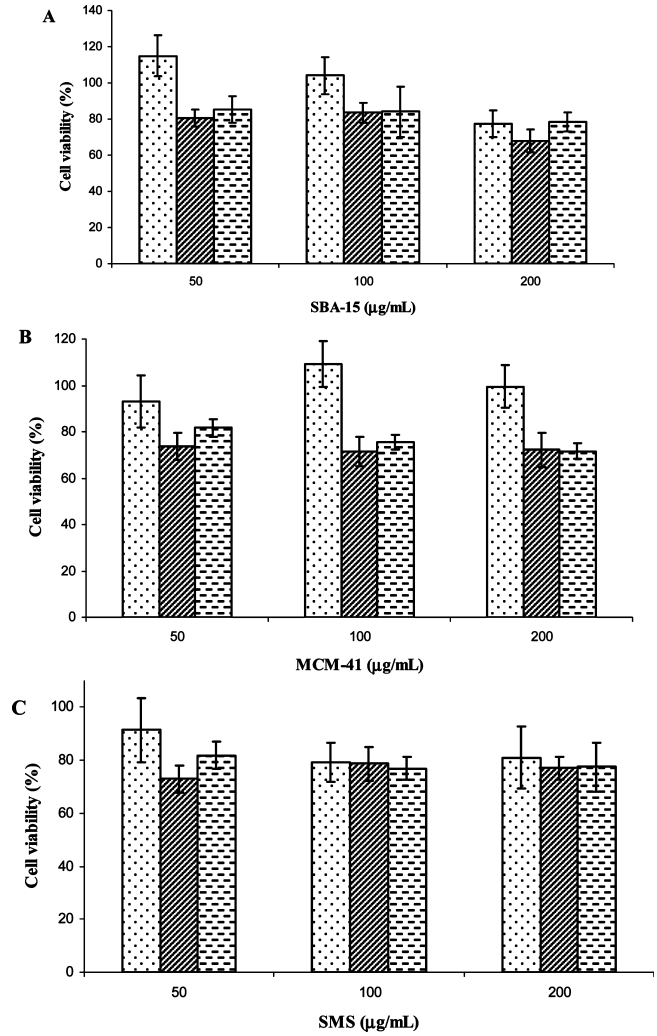

Figure 2. Jurkat cell viability due to the treatment of various silica nanoparticles: (A) SBA-15, (B) MCM-41, and (C) SMS, at different dosages employed (as indicated). Bars filled with dots, lines, or dashes represent the cell viability at different incubation times of 3, 27, or 51 h, respectively. Standard deviations were obtained from $n = 6$ measurements.

200 μg/mL, SBA-15 executed an immediate toxicity on Jurkat cells (~20% dead). At 27 h, both 50 and 100 μg/mL SBA-15 had an increasing impact on cell viability, as 200 μg/mL SBA-15 caused ~30% cell death. This result suggested that the cytotoxicity of SBA-15 on Jurkat cells was dose-dependent as well as time-dependent. At 51 h of incubation, neither 50 nor 100 μg/mL SBA-15 exerted an evident toxicity on Jurkat cells, albeit the fluctuations in cell viability were quite large, while the dosage of 200 μg/mL exhibited a profound toxicity. Moreover, during an incubation for a total of 51 h, the doubling time was found to be (25.5 ± 1.8) h in untreated cells, (33.0 ± 3.1) h in 50 μg/mL SBA-15-treated cells, (30.5 ± 4.8) h in 100 μg/mL SBA-15-treated cells, and (25.2 ± 1.4) h in 200 μg/mL SBA-15-treated cells. Hence, the inhibitory effect of SBA-15 particles on Jurkat cell proliferation was small.

Figure 2B and Table 2 show the cytotoxicity and cell viability due to the incubation with 50, 100, or 200 μg/mL MCM-41 nanoparticles. Clearly, at all dosages applied, MCM-41 nanomaterials had no observable effect on Jurkat cell viability during 3 h of incubation. This is consistent with our previous findings that MCM-41 had no significant inhibition on cell respiration in the same period of incubation, whereas SBA-15 impaired cellular respiration in a dose-dependent manner (*38*). However, at 27 h, cell viability dropped significantly in the three dosages

Table 2. Cell Viability in the Presence of Different Concentrations of Silica Nanoparticles[a]

	dosage (μg/mL)	3 h incubation	*p*-value	27 h incubation	*p*-value	51 h incubation	*p*-value
SBA-15	50	114.9 ± 11.2	0.16	80.7 ± 4.7	0.02	85.2 ± 7.5	0.13
	100	104.1 ± 10.2	0.62	83.4 ± 5.5	0.03	84.0 ± 14.0	0.32
	200	77.5 ± 7.3	<0.01	67.9 ± 6.2	<0.001	78.5 ± 5.3	<0.01
MCM-41	50	92.9 ± 11.2	0.02	73.7 ± 6.0	<0.001	81.6 ± 3.7	<0.003
	100	109.4 ± 9.9	0.51	71.5 ± 6.4	<0.006	75.4 ± 3.1	<0.002
	200	99.5 ± 9.2	0.06	72.2 ± 7.4	<0.008	71.7 ± 3.4	<0.0004
SMS	50	91.4 ± 12.1	0.11	72.9 ± 5.3	<0.003	81.9 ± 5.2	<0.008
	100	79.3 ± 7.4	<0.004	78.7 ± 6.4	<0.007	76.9 ± 4.4	<0.0003
	200	80.9 ± 11.7	0.03	77.1 ± 4.2	<0.004	77.4 ± 9.1	<0.02

[a] Eight thousand Jurkat cells/well were plated and immediately treated with nanoparticles. SBA-15, MCM-41, and SMS of three concentrations (50, 100, and 200 μg/mL, respectively) were added. Plates were then incubated at 37 °C with 5% CO_2 for 3 days. Each day (i.e., 0, 24, and 48 h), plates were taken, followed by adding 10 μL of WST-8 agent and incubated for another 3 h. The absorbance was then measured at 450 nm using a microplate reader. Cell viability under each condition, compared to that of the untreated cells, was summarized.

applied. It was, therefore, concluded that 50−200 μg/mL MCM-41 had a remarkable toxicity on Jurkat cells. Furthermore, this toxicity tended to be independent of particle amount over a long period of exposure. The cell viability on the next day remained nearly unchanged or revealed a minute recovery, implying a limited cytotoxicity of MCM-41. The calculations with respect to the cell doubling time illustrated that 50 μg/mL MCM-41 prolonged Jurkat cell replication by (2.8 ± 2.8) h (i.e., statistically zero), 100 μg/mL by (10.2 ± 2.4) h, and 200 μg/mL by (8.5 ± 2.5) h. Taken together, there was no recognized cell death by MCM-41 treatment unless there was a long exposure (after one-day), although cell growth was eventually inhibited in a dose-dependent manner.

Jurkat cells incubated with 50, 100, or 200 μg/mL SMS nanoparticles for different incubation times (Figure 2C and Table 2) displayed various cell viabilities over time. During the first 3 h of incubation, except at a dosage of 50 μg/mL, the solid SMS nanoparticles were lethal to Jurkat cells. One day later, SMS at 50−200 μg/mL had an appreciable toxicity on Jurkat cells. This toxicity appeared acute for high doses of SMS, but chronic for low doses. Moreover, once the toxicity became evident, it turned out to be dose-independent. With one more day of incubation, it exhibited a constant cell death in the presence of SMS. Cell doubling time was then calculated, yielding (27.8 ± 2.7) h for 50 μg/mL, (26.1 ± 1.3) h for 100 μg/mL, and (26.4 ± 3.4) h for 200 μg/mL SMS-treated cells. Essentially, SMS had no inhibitory effect on cell growth.

Being an efficient anticancer drug, cisplatin induced cell death through caspase-dependent apoptosis (*45, 46*). In Jurkat cells, experiments done within the same incubation period under treatment of 40 μM cisplatin showed a cell viability of (75.1 ± 9.5) % in the first day and dropped to zero in the second day. As for the concerns that the cytotoxicity induced by nanoparticles might come from the physical wrappings or surroundings of particles on cell surfaces, experiments by laying down nanoparticles first into plates and later gently adding cell suspensions were performed. Similar results were obtained, which became in line with the recent report by Hudson et al. (*40*). Considering the possible interference or adsorption of WST-8 by silica nanoparticles, we realized that in the cell-free medium, various types of particles (SBA-15, MCM-41, and SMS) yield different light absorbance, on the basis of the same mass addition. However, with the same particle present, the differences in absorbance from different concentrations (50, 100, or 200 μg/mL) were negligible.

To investigate whether the cytotoxicity of the nanoparticles was dependent on cell type, similar experiments using adherent SK-N-SH cells that derived from human neuroblastma were conducted (Figure 3 and Table 3). At 3 h, SBA-15 nanomaterials exhibited notable toxicity on SK-N-SH cells in a dose-dependent manner, although they nearly had no effect on cells at a low dosage of 50 μg/mL. This cytotoxicity appeared similar to that on Jurkat cells. Twenty-four hours later, neither 50 nor 100 μg/mL SBA-15 showed an inhibitory effect on cell viability, whereas the cytotoxicity of 200 μg/mL SBA-15 remained constant. This result implied that the injury of SBA-15 nanoparticles on SK-N-SH cells was dose-dependent and that cells could recover from injuries due to a relatively low dosage. At

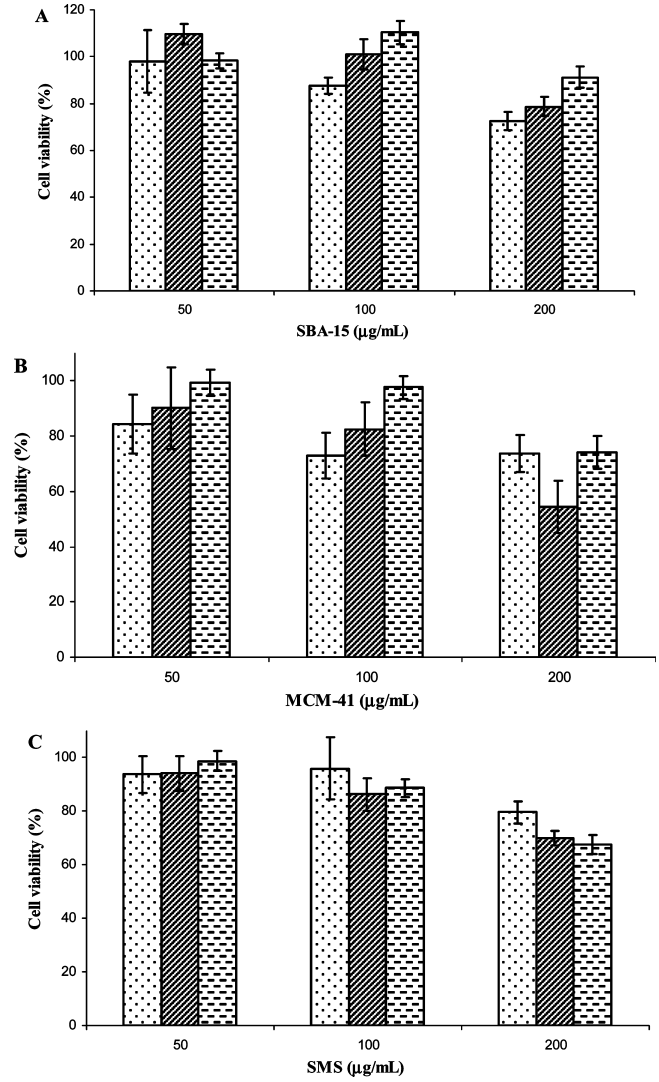

Figure 3. SK-N-SH cell viability due to the treatment with various silica nanoparticles: (A) SBA-15, (B) MCM-41, and (C) SMS, at different dosages employed (as indicated). Bars filled with dots, lines, or dashes represent the cell viability at different incubation times of 3, 27, or 51 h, respectively. Standard deviations were obtained from $n = 6$ measurements.

Table 3. SK-N-SH Cell Viability due to the Treatment with SBA-15, MCM-41, and SMS[a]

	dosage (μg/mL)	3 h incubation	*p*-value	27 h incubation	*p*-value	51 h incubation	*p*-value
SBA-15	50	98.0 ± 13.3	0.99	109.8 ± 4.3	<0.003	98.2 ± 3.3	0.65
	100	87.6 ± 3.4	<0.008	100.9 ± 6.4	0.46	110.3 ± 4.9	0.003
	200	72.4 ± 4.0	<0.0002	78.8 ± 4.0	<0.003	91.1 ± 4.5	0.05
MCM-41	50	84.5 ± 10.7	0.02	90.1 ± 14.7	0.46	99.4 ± 4.9	0.21
	100	72.9 ± 8.3	0.005	82.6 ± 9.6	0.07	97.7 ± 4.1	0.68
	200	73.8 ± 6.7	<0.001	54.5 ± 9.5	0.003	74.2 ± 5.8	0.004
SMS	50	93.8 ± 6.8	0.29	94.2 ± 6.6	0.66	98.8 ± 3.6	0.005
	100	96.0 ± 11.6	0.83	86.3 ± 6.2	0.07	88.7 ± 3.5	0.02
	200	79.6 ± 4.0	<0.002	70.0 ± 2.8	<0.0004	67.7 ± 3.5	<0.0004

[a] Six thousand SK-N-SH cells per well were plated 24 h before the addition of nanoparticles. Time zero corresponds to the addition of three concentrations (50, 100, and 200 μg/mL, respectively) of SBA-15, MCM-41, and SMS. At each day (i.e., 0, 24, and 48 h), plates were taken, followed by the addition of 10 μL of WST-8 agent, and incubated for another 3 h. The absorbance was then measured at 450 nm using a microplate reader. Cell viability under each condition, compared to that of the untreated cells, was summarized.

51 h of incubation, as 50 and 100 μg/mL SBA-15 continued a minimal cytotoxicity on SK-N-SH cells, the cell viability under treatment of 200 μg/mL SBA-15 denoted a recovery over time. In addition, 50−200 μg/mL SBA-15 did not substantially lengthen the doubling time of SK-N-SH cells (results not shown). Compared to the toxicity on Jurkat cells, SBA-15 had a similar toxic effect on SK-N-SH cells, which was dependent on the concentrations of nanoparticles. However, differing from Jurkat cells, the SK-N-SH cells showed more resistance to the treatment of SBA-15, as the cytotoxicity caused by high dosage to the latter decreased over time.

MCM-41 nanomaterials also showed toxicity to SK-N-SH cells during the short exposure (3 h) in a manner similar to that of SBA-15 (Figure 3B and Table 3). However, this toxicity was different from that on Jurkat cells, where MCM-41 had no observable effect on cell viability at the same incubation period. At 27 h, the toxicity induced by 50−100 μg/mL MCM-41 was slightly decreased over time. However, the toxicity persisted when cells were incubated with 200 μg/mL MCM-41. Furthermore, the viability at 51 h suggested a full recovery in 50 and 100 μg/mL MCM-41-treated cells. A partial recovery was also found in 200 μg/mL MCM-41-treated cells, although cell death remained evident. All of these results implied that there was a changeable and recoverable toxicity of MCM-41 on SK-N-SH cells. The calculations of cell doubling time revealed that 50−200 μg/mL MCM-41 did not essentially prolong SK-N-SH cell duplication (results not shown). Obviously, compared to the results obtained from the study on Jurkat cells, MCM-41 had a more acute toxicity on SK-N-SH cells; the cells, however, eventually become more resistant to death with the MCM-41 treatment.

Viability of SK-N-SH cells, incubated with 50, 100, or 200 μg/mL SMS nanoparticles (Figure 3C and Table 3), indicated that silica nanoparticles with solid cores were not toxic to SK-N-SH cells unless a high dosage of 200 μg/mL was applied at 3 h exposure. One day later, at a dosage of 50 μg/mL, SMS remained harmless to SK-N-SH cell viability, while 100−200 μg/mL SMS had increasing cytotoxicity. Finally, the experiment at 51 h indicated that SMS treatment exhibited a constant toxicity on SK-N-SH cells, which appeared acute for high doses of SMS but chronic for low doses. SMS had no inhibitory effect on growth SK-N-SH cells because the cell doubling time under 50−200 μg/mL SMS treatment showed no statistical difference compared to that of the cells that were not treated with SMS (results not shown).

Similar experiments, incubating SK-N-SH cells with 40 μM cisplatin, revealed a viability of (84.0 ± 7.4) % at 3 h. This value was dropped to (5.1 ± 2.1) % at 27 h and became completely zero at 51 h. Therefore, cisplatin executed cell death on neuroblastoma cells similar to that on Jurkat cells. A bright field microscopy was utilized for observations of SK-N-SH cells under treatment of 200 μg/mL nanoparticles or 40 μM cisplatin during a 24-h incubation. The images were then taken and shown in Figure 4. In cells incubated with various nanoparticles, SBA-15 (Figure 4B), MCM-41 (Figure 4C), or SMS (Figure 4D), the surfaces of the cells were partially covered or surrounded by particles. Compared to the untreated cells (Figure 4A), the morphology of the cells was not changed after treatment with nanoparticles, confirming a limited cytotoxicity that was not induced by physical wrapping of nanomaterials. Simultaneously, the majority of cells tended to be dying because of the exposure to cisplatin (Figure 4E), forming groups of apoptotic bodies.

3.3. Cytotoxicity of Functionalized Silica Nanoparticles. To further explore the effect of surface functionalization on induced cytotoxicity, we functionalized silica nanoparticles with quaternary amine groups (noted as SBA-N, MCM-N, and SMS-N) and used them in toxicity studies (Figure 5). Contrary to the ungrafted SBA-15, SBA-N nanomaterials barely showed noticeable toxicity to Jurkat cells after a total of 51 h incubation. In other words, amination largely neutralized the toxicity of SBA-15 nanoparticles on Jurkat cells. The cell doubling time was also found to be (24.4 ± 1.5) h in untreated cells and (24.7 ± 1.4) h in 50 μg/mL, (24.5 ± 1.5) h in 100 μg/mL, and (22.3 ± 1.0) h in 200 μg/mL SBA-N treated cells. Hence, the effect of amine-functionalized SBA nanoparticles on cell growth was negligible.

The toxicity of MCM-N on Jurkat cells (Figure 5B and Table 4) with a concentration of 50−200 μg/mL showed little or no cytotoxicity after a total of 27 h incubation. Within statistical errors, the cell viability on the next day (i.e., 51 h) kept unchanged, confirming a perfect biocompatibility of MCM-N particles without apparent cytotoxicity. The calculations with respect to the cell doubling time revealed that there was no inhibition of cell growth under 50−200 μg/mL MCM-N incubation (results not shown). Thus, amination counteracted the cytotoxicity of MCM-41 in the same manner as it did to SBA-15.

In the presence of various concentrations of SMS-N (Figure 5C and Table 4), the viability of Jurkat cells decreased significantly after a short incubation (3 h), independent of the doses applied. This instant cell damage lasted for another 48 h. Therefore, it implied that once treated, SMS-N induced a rapid as well as constant toxicity to Jurkat cells. Compared to the effect of SMS on the same cell line, the cytotoxic profiles of SMS-N nanoparticles were very similar. That is, amination failed in rescuing Jurkat cells from injury caused by silica spheres. The calculated cell doubling times for SMS-N were (24.3 ± 2.2) h, (22.6 ± 1.2) h, and (22.4 ± 2.0) h for 50, 100, and 200 μg/mL SMS-N treatments, respectively, suggesting that there was no effect on cell proliferation due to the treatment of SMS-N particles.

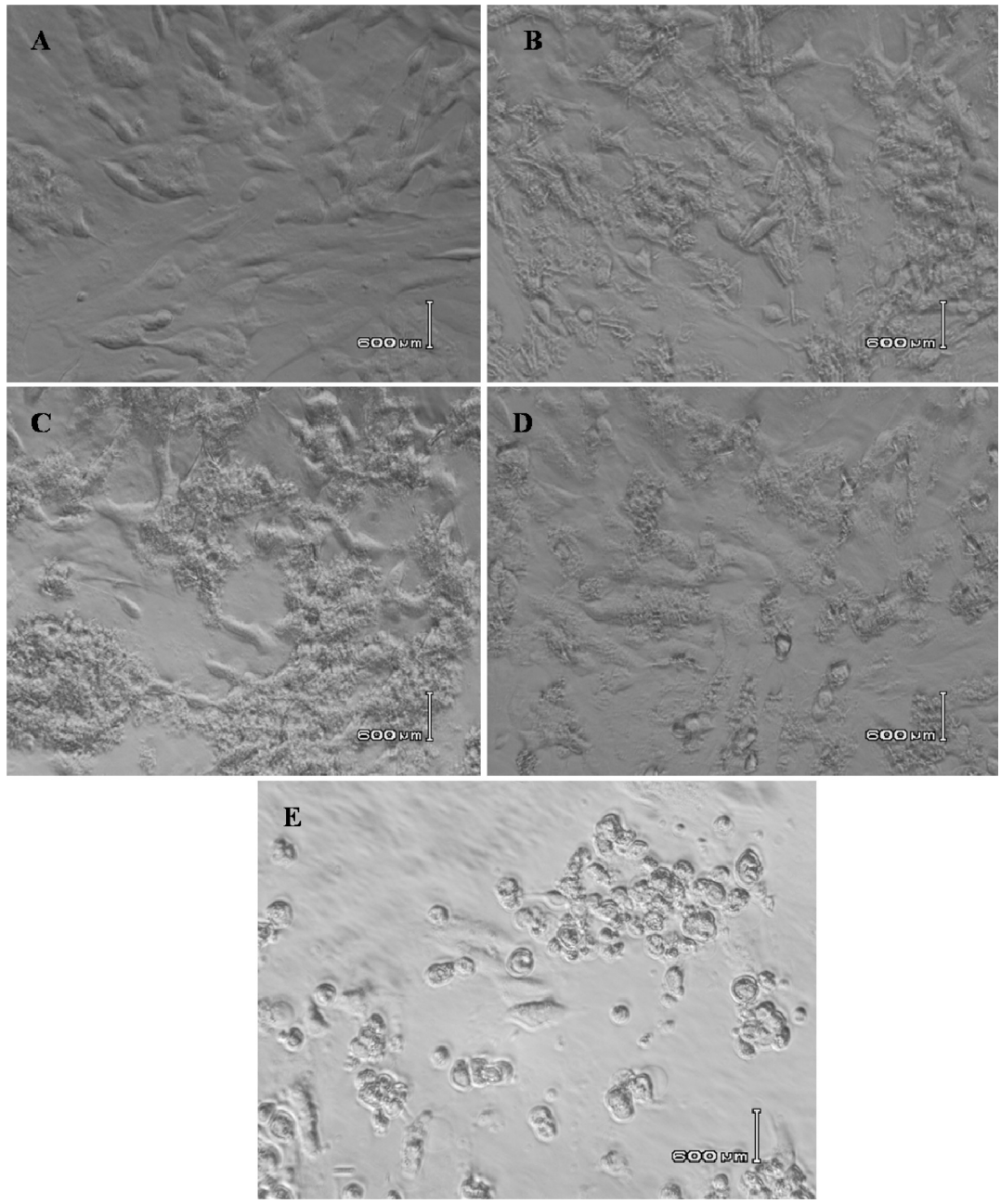

Figure 4. SK-N-SH cell images under bright field microscope after 24 h of incubation without (A) or with various silica nanoparticles: (B) SBA-15, (C) MCM-41, and (D) SMS. As a reference, SK-N-SH cells treated with 40 μM cisplatin are also shown in E. Scale bars indicate a size of 600 μm.

The toxicity of MSN-N and SMS-N under different conditions during various incubation times on SK-N-SH cells was also measured (Figure 6 and Table 5). SBA-N showed a small toxicity after 3 h exposure to SK-N-SH cells, similar to that on Jurkat cells. Cytotoxicity induced by SBA-N particles after 27 h of incubation increased in a dose-dependent manner. At 51 h, the treatment of the cells with 50−200 μg/mL SBA-N resulted in persistent or slightly decreased cell viability. Therefore, SBA-N had a time-dependent and concentration-dependent toxicity on SK-N-SH cells. Moreover, 50−200 μg/mL SBA-N substantially prolonged the doubling time of SK-N-SH cells. It was (41.7 ± 3.1) h for the untreated cells to replicate, which was delayed under the treatment of 50 μg/mL SBA-N by (6.9 ± 2.7) h, 100 μg/mL SBA-N by (4.3 ± 2.7) h, and 200 μg/mL SBA-N by (20.8 ± 3.3) h. Thus, compared to its toxicity to Jurkat cells, SBA-N appeared more toxic to SK-N-SH cells. More specifically, this enhanced cytotoxicity clearly resulted from amination since SK-N-SH cells showed more resistance to the treatment of ungrafted SBA-15.

The cytotoxicity of MCM-N nanoparticles on SK-N-SH cells is shown in Figure 6B. After 3 h of exposure, MCM-N nanomaterials were safe to SK-N-SH cells at concentrations of 50−200 μg/mL, which was quite different from MCM-41 samples that had a considerable toxicity on SK-N-SH cells during the same incubation period. At 27 h, cell death became noticeable in cells treated by 200 μg/mL MCM-N particles but not in cells treated by a lower amount of MCM-N. This dose-dependent toxic manner remained similar at 51 h, as no toxicity was observed in 50−100 μg/mL MCM-N-treated cells. However, 200 μg/mL MCM-N led to partial cell death. These results implied a tolerable toxicity of MCM-N by SK-N-SH cells. Moreover, the cell doubling time revealed that 50−100 μg/mL MCM-N had statistically no influence on cell duplication, but 200 μg/mL MCM-N prolonged the doubling time by (10.8 ±

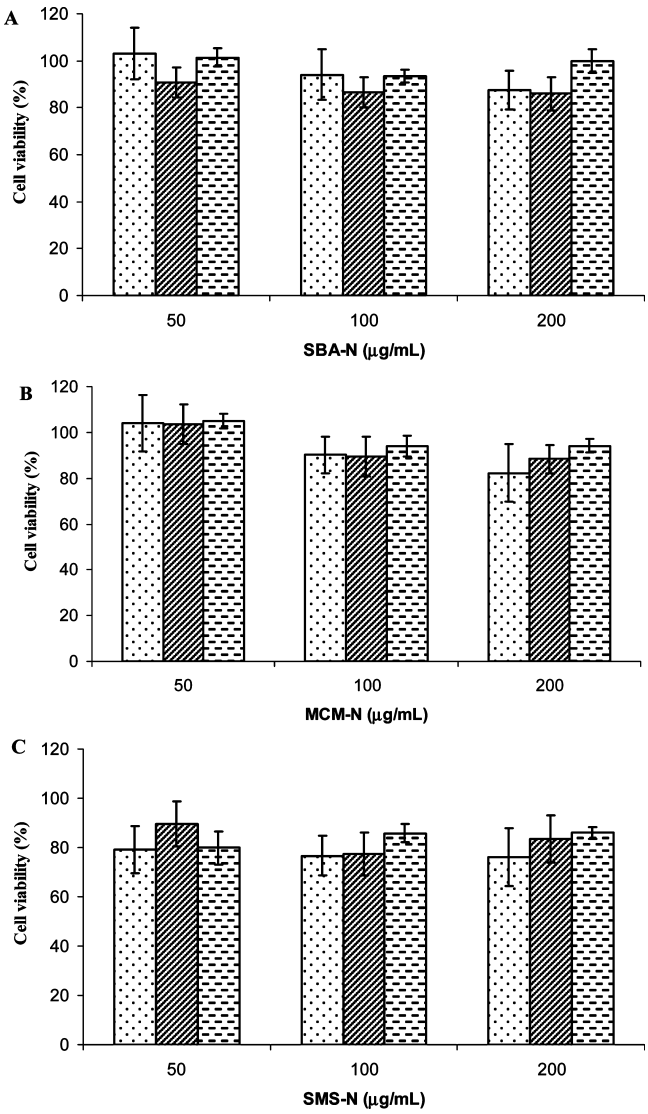

Figure 5. Jurkat cell viability due to the treatment of various aminated silica nanoparticles: (A) SBA-N, (B) MCM-N, and (C) SMS-N, at different dosages employed (as indicated). Bars filled with dots, lines, or dashes represent the cell viability at different incubation times of 3, 27, or 51 h, respectively. Standard deviations were obtained from $n = 6$ measurements.

4.5) h. Hence, for SK-N-SH cells, a relatively high dosage of MCM-N inhibited cell growth and induced cell death.

Finally, the cytotoxicity of SMS-N on SK-N-SH cells was investigated (Figure 6C). At 3 h of incubation, a fluctuation in cell viability with the addition of nanoparticles reflected a variable but limited toxicity. SMS-N induced a similar dosage-independent toxicity on SK-N-SH cells after 24 h as it did on Jurkat cells. Furthermore, the earlier fluctuation in cytotoxicity diminished over time, allowing us to determine the material's effect on cell death. At a total of 51 h of incubation time, SMS-N particles had a trivial impact on SK-N-SH cell viability. Further calculations of the doubling time revealed no difference between untreated and treated SK-N-SH cells (results not shown). All of these results demonstrated that functionalization of quaternary amines on the outer surface of SMS made silica spheres less toxic to SK-N-SH cells and caused no effect on cell growth.

3.4. Cellular Uptake of Silica Nanoparticles. The cellular uptake of the silica nanoparticles in cancer cell lines were also investigated using transmission electron microscopy. If we assume all of the nanomaterials studied above to be strictly spherical in shape, a particle with a diameter of 300 nm and a density of 2.2 g/cm^3 (SiO_2) has a mass of 3.1×10^{-14} g and a volume of 1.4×10^{-14} mL. Thus, 200 μg/mL corresponds to 6.5×10^9 particles in 1 mL addition. When we plated 8000 Jurkat cells per well (100 μL), there were $\sim 8.0 \times 10^4$ particles per cell. Assuming the mean volume of one Jurkat cell as 1.7×10^{-13} L (*38*), i.e., 1.2×10^4 times that of a single particle and assuming a spherical shape, we calculated that the surface area of a Jurkat cell is $\sim 1.48 \times 10^{-10}$ m^2 or $\sim$525 times that of one particle. Hence, the particles added, if all stay in contact with cells in solution, represent 6.7 times the volume or 153 times the area of the cells. However, it is not clear yet whether the particles are stuck to the cell surface, internalized by cells, or both. Thus, our next effort was made to collect evidence in support of or to discount endocytosis of these silica nanoparticles.

Jurkat cells (0.5×10^6 cells per mL) were incubated with 200 μg/mL nanoparticles (SBA-5, MCM-41, and SMS, grafted with or without quaternary amines) for 1 h and kept gently stirring. Cell suspensions (1.5 mL) were then collected, processed, microtomed, and visualized by TEM. As shown in Figure 7, during 1 h of incubation at 37 °C, Jurkat cells swallowed SBA-15 (Figure 7A) and MCM-41 (Figure 7B) by engulfing the particles with their cell membranes. For SBA-15 nanoparticles, the cytoplasm membranes were more likely to fold inward in order to absorb the material from outside, suggesting a possible receptor-mediated endocytosis. Normally, this internalization of extracellular objects would form cytoplasmic vesicles that are coated by cytosolic proteins. Those particles could travel inside the cytoplasm or even commute between nuclei and cytosols, as shown in Figure 7A (lower panel). An internalized SBA-15 particle was seized crossing the nuclear membrane. However, the mechanism of endocytosis of MCM-41 particles could be very different. Figure 7B freezes the moment when MCM-41 nanoparticles were ingested by Jurkat cells, showing a typical process of phagocytosis. The cell membranes clearly folded around MCM-41 particles,

Table 4. Toxicity of MSN-N and SMS-N on Jurkat Cells[a]

	dosage (μg/mL)	3 h incubation	*p*-value	27 h incubation	*p*-value	51 h incubation	*p*-value
SBA-N	50	102.9 ± 11.0	0.60	90.7 ± 6.4	0.05	101.4 ± 3.9	0.26
	100	94.0 ± 10.8	<0.003	86.4 ± 6.4	0.07	93.5 ± 2.7	<0.008
	200	87.5 ± 8.4	0.04	86.0 ± 7.1	0.07	99.8 ± 5.0	0.93
MCM-N	50	103.9 ± 12.2	0.62	103.7 ± 8.7	0.35	104.8 ± 3.2	0.08
	100	90.2 ± 8.0	0.09	89.4 ± 8.7	0.20	94.2 ± 4.6	0.07
	200	82.3 ± 12.6	0.09	86.0 ± 6.2	0.04	94.2 ± 2.8	0.07
SMS-N	50	79.2 ± 9.5	0.003	89.7 ± 9.1	0.11	79.8 ± 6.8	0.01
	100	76.7 ± 8.2	<0.0001	77.3 ± 8.8	0.01	85.8 ± 3.8	0.001
	200	76.1 ± 11.8	<0.007	83.3 ± 9.6	0.10	85.9 ± 2.5	0.0003

[a] Eight thousand Jurkat cells/well were plated and immediately treated with nanoparticles. SBA-N, MCM-N, and SMS-N of three concentrations (50, 100, and 200 μg/mL, respectively) were added. Plates were then incubated at 37 °C with 5% CO_2 for 3 days. Each day (i.e., 0, 24, and 48 h), plates were taken, followed by the addition of 10 μL of WST-8 agent, and incubated for another 3 h. The absorbance was then measured at 450 nm using a microplate reader. Cell viability under each condition, compared to that of the untreated cells, was summarized.

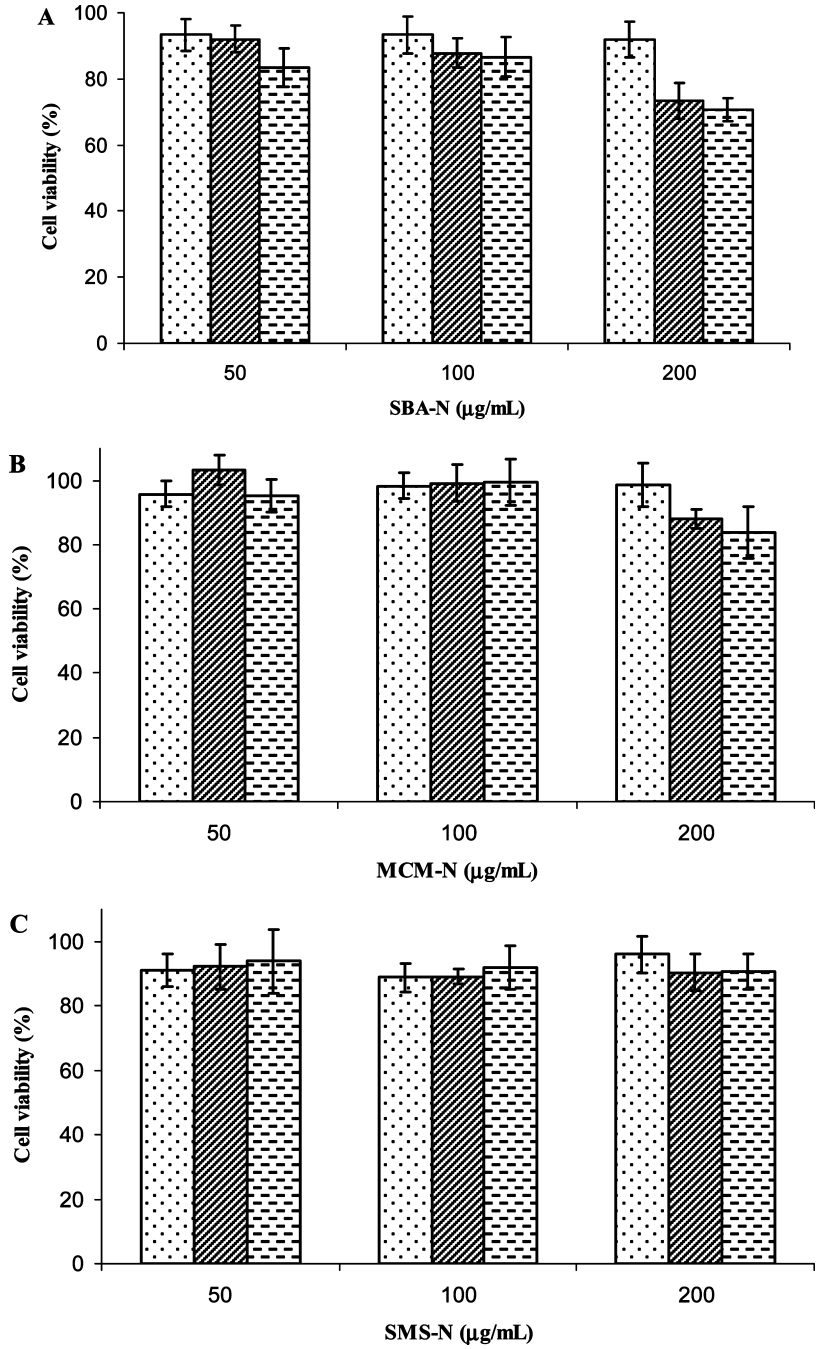

Figure 6. SK-N-SH cell viability due to the treatment of various aminated silica nanoparticles: (A) SBA-N, (B) MCM-N, and (C) SMS-N, at different dosages employed (as indicated). Bars filled with dots, lines, or dashes represent the cell viability at different incubation times of 3, 27, or 51 h, respectively. Standard deviations were obtained from $n = 6$ measurements.

Table 5. Toxicity of MSN-N and SMS-N under Different Conditions during Various Incubation Times on SK-N-SH Cells[a]

	dosage (μg/mL)	3 h incubation	*p*-value	27 h incubation	*p*-value	51 h incubation	*p*-value
SBA-N	50	93.3 ± 4.9	0.05	92.0 ± 4.1	0.04	83.3 ± 5.8	0.04
	100	93.3 ± 5.7	0.04	87.7 ± 4.5	0.006	86.6 ± 5.9	0.04
	200	92.0 ± 5.4	0.02	73.3 ± 5.4	0.001	70.6 ± 3.6	0.002
MCM-N	50	95.7 ± 3.9	0.12	103.2 ± 4.8	0.09	95.1 ± 5.0	0.22
	100	98.3 ± 4.0	0.27	99.1 ± 5.7	0.81	99.2 ± 7.2	0.88
	200	98.7 ± 6.7	0.59	88.1 ± 2.9	<0.001	83.8 ± 8.0	0.07
SMS-N	50	90.9 ± 5.0	0.04	92.1 ± 6.9	0.18	93.9 ± 9.9	0.43
	100	88.8 ± 4.4	0.002	89.0 ± 2.4	0.001	91.9 ± 6.9	0.04
	200	95.9 ± 5.7	0.18	90.4 ± 5.5	0.05	90.8 ± 5.5	0.04

[a] Six thousand SK-N-SH cells per well were plated 24 h before the addition of nanoparticles. Time zero corresponds to the addition of three concentrations (50, 100, and 200 μg/mL, respectively) of SBA-N, MCM-N and SMS-N. At each day (i.e., 0, 24, and 48 h), plates were taken, followed by the addition of 10 μL of WST-8 agent, and incubated for another 3 h incubation. The absorbance was then measured at 450 nm using a microplate reader. Cell viability under each condition, compared to that of the untreated cells, was summarized.

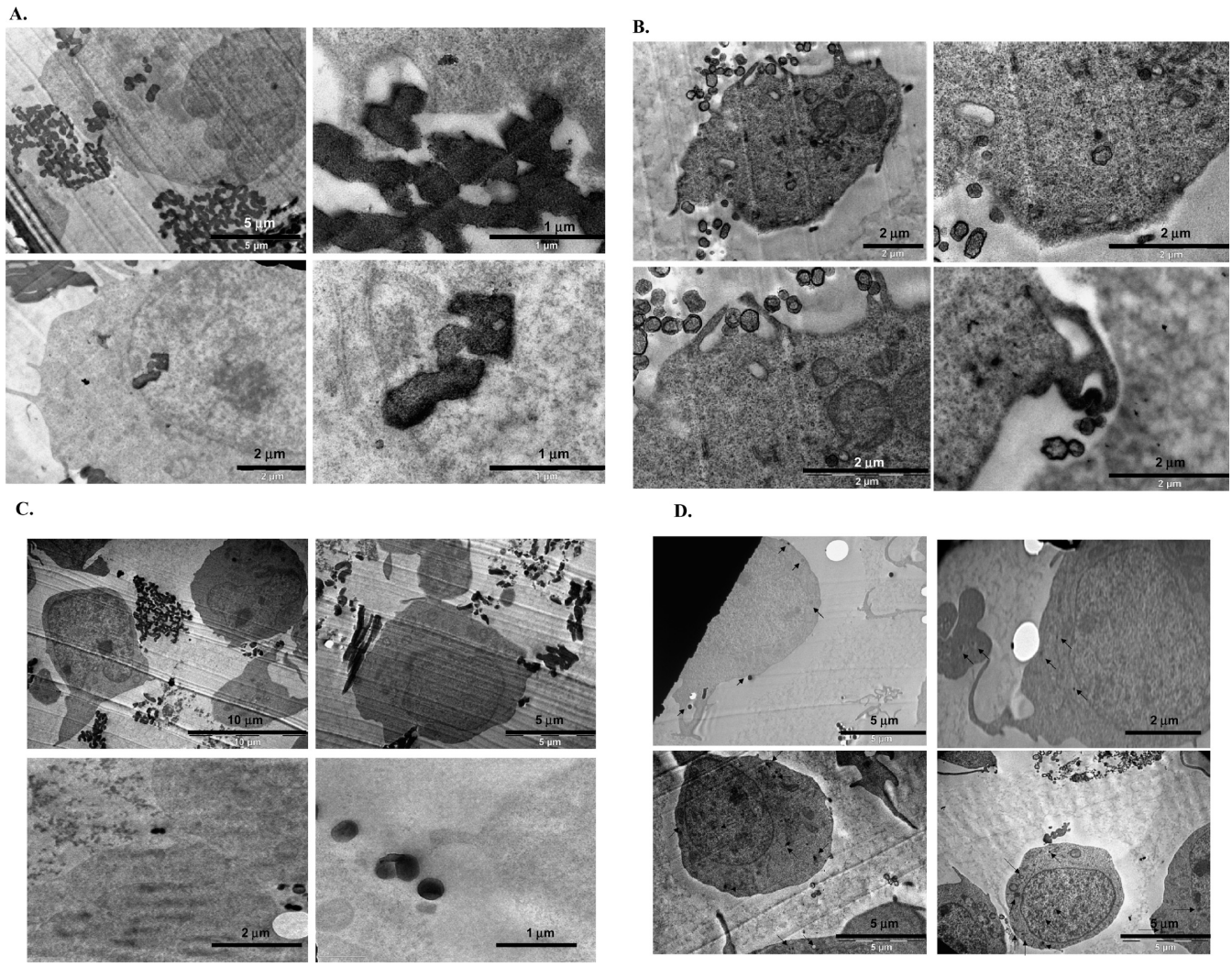

Figure 7. TEM images that visualized the uptake of silica nanoparticles by Jurkat cells. (A) Endocytosis of SBA-15. The cytoplasm membranes are inclined to fold with an intension to absorb the material from outside. In addition, an internalized SBA-15 nanoparticle was observed penetrating the nuclear membrane. (B) Endocytosis of MCM-41. Particles are ingested by cells as cell membranes hug around MCM-41 nanoparticles, forming a pseudopodium. (C) Endocytosis of SBA-N (upper panel) or MCM-N (lower panel). No efficient endocytosis can be observed, as particles stay outside of cells in the medium. (D) Endocytosis of SMS (upper panel) or SMS-N (lower panel). Internalized solid nanoparticles are indicated by arrows.

forming a pseudopodium; this was a natural defense of the cell against unwanted objects, but unfortunately, it failed here. The hexagonal packing of MCM-41 nanoparticles can be easily observed inside the cells. However, there was much less efficient endocytosis observed in cells treated with 200 μg/mL either SBA-N (upper panel, Figure 7C) or MCM-N (lower panel, Figure 7C). The positively charged groups on the mesoporous nanoparticles, produced by grafting of the quaternary amines, were inclined to bind the negatively charged cell membrane instead of bringing the materials into the cytoplasm. This actual failure in endocytosis protected the cells from serious injury, although the physical damage of the lipid membrane might still occur.

The endocytotic processes for SMS (upper panel) and SMS-N (lower panel) are shown in Figure 7D. Basically, the internalization of solid spherical particles was as efficient as that of mesoporous particles, seeing that ingested silica spheres were dissipated inside the cells. Close observations along the cell membrane suggested that the solid-cored spheres diffused across the cellular boundary, causing severe impairment to the intracellular organelles and therefore promoting cell death. Compared to that of SMS, the intracellular distribution of SMS-N suggested that these aminated silica spheres were more likely to accumulate inside the nucleus, which became in line with the positive charge and concrete nature of SMS-N particles. Given the fact that a small amount of SMS-N (50 μg/mL) could immediately execute more serious cytotoxicity than SMS did, quaternary amines tended to facilitate the intracellular transportation of silica spheres, which previously failed the mesoporous particles in entering cells. This observed difference in endocytosis between the aminated mesoporous nanoparticles and silica nanospheres can also be attributed to the possible difference in the degree of interaction between the nanomaterials and the cell membranes via such forces as capillary action between the mesopores or the materials and the cell membranes, whose strength may depend on the existence of pores on the material nature and the pore sizes, if any.

4. Conclusions

Silica nanomaterials, including mesoporous MCM-41 and SBA-15, and solid-cored spheres (SMS), and their ammonium functionalized counterparts were synthesized, and their cytotoxicities on adherent and suspended cells were investigated. In Jurkat cells, SBA-15 exhibited cytotoxicity in a time-dependent and concentration-dependent manner, while MCM-

41 showed cytoxicity in a time-dependent but concentration-independent manner. No significant cell death was detected when treating the same cells with aminated SBA-N or MCM-N samples. That is, positively charged quaternary amines prevented cellular injury from mesoporous nanoparticles. The endocytosis study confirmed this effect, where the effective internalization of MSN but not MSN-N was observed. SK-N-SH cells appeared more resistant to the treatment of MSN, unaminated or aminated. Incubation with either SBA-15 or MCM-41 over time showed a recovery in cell viability, while exposure to MSN-N particles only induced a noticeable cell death at longer incubation with a high dosage of 200 μg/mL. MSN-N (but not MSN) particles inhibited SK-N-SH (but not Jurkat) cell doubling time in a dose-dependent manner. Whether aminated or not, silica spheres had an instant and constant toxicicty on Jurkat cells. TEM images revealed an effective endocytosis of SMS and SMS-N, although SMS-N appeared to be more likely to enter the nucleus. For solid silica spheres, although the positive charge due to amination still made cellular uptake less efficient, the rigid nature of these particles dismantled cells in a different manner compared to that of their MSN counterparts. Thus, it can be concluded that the cytotoxicity of silica nanoparticles is particle-dependent as well as cell-type dependent. Moreover, this dependency further varied with incubation time and particle dosage. This was primarily associated with the endocytotic efficiency of nanoparticles, which was found to depend largely on their chemical property, such as the grafting of organic groups. An excellent work has been recently reported on the cytotoxicity and biocompatibility of MCM-41, SBA-15, and mesocellular foam (MCF) on *in vitro* mammalian cells as well as *in vivo* mouse models (*40*). The results indicated that mesoporous silicates showed a significant degree of toxicity at high concentrations. Although it was previously proposed that the toxicity of the materials might be mitigated by modification of the materials (*40*) and while our work was consistent with some of these results, our study here was the first ever to illustrate the effect of the functionalization of mesoporous materials on their cytotoxicity both in dose- and cell type-dependent manners on adherent and suspended cells.

Acknowledgment. T.A. thanks the US National Science Foundation (NSF), contract Nos. CHE-0645348 and NSF-DMR 0804846, for the partial financial support of this work. B.B.T. and Z.T. are grateful to The Arnold Family for supporting part of this research by Paige's Butterfly Run. Z.T. is currently a Japan Society for Promotion of Science postdoctoral fellow in Graduate School of Medicine, Kyoto University, Japan.

Supporting Information Available: Experimental details, N_2 BET gas adsorption isotherms. and BJH pore-size distributions of the nanomaterials investigated. This material is available free of charge via the Internet at http://pubs.acs.org.

References

(1) Soppimath, K. S., Aminabhavi, T. M., Kulkarni, A. R., and Rudzinski, W. E. (2001) Biodegradable polymeric nanoparticles as drug delivery devices. *J. Controlled Release 70*, 1–20.

(2) Blumen, S. R., Cheng, K., Ramos-Nino, M., Taatjes, D., Weiss, D., Landry, C. C., and Mossman, B. T. (2007) Unique uptake of acid-prepared mesoporous spheres by lung epithelial and mesothelioma cells. *Am. J. Respir. Cell Mol. Biol. 36*, 333–342.

(3) Solberg, S. M., and Landry, C. C. (2006) Adsorption of DNA into mesoporous silica. *J. Phys. Chem. B 110*, 15261–15268.

(4) Brigger, I., Dubernet, C., and Couvreur, P. (2002) Nanoparticles in cancer therapy and diagnosis. *Adv. Drug Delivery Rev. 54*, 631–651.

(5) Rhaese, S., von Briesen, H., Rübsamen-Waigmann, H., Kreuter, J., and Langer, K. (2003) Human serum albumin- derived nanoparticles for gene delivery. *J. Controlled Release 992*, 199–208.

(6) Sokolov, I., and Naik, S. P. (2008) Novel fluorescent silica nanoparticles: Towards ultrabright silica nanoparticles. *Small 4*, 934–939.

(7) Ispas, C., Sokolov, I., and Andreescu, S. (2009) Enzyme functionalized mesoporous silica for bioanalytical applications. *Anal. Bioanl. Chem. 393*, 543–554.

(8) Ong, Q., and Sokolov, I. J. (2007) Attachment of nanoparticles to the AFM tips for direct measurements of interaction between a single nanoparticle and surfaces. *Colloid Interf. Sci. 310*, 385–390.

(9) Slowing, I. I., Trewyn, B. G., Giri, S., and Lin, V. S.-Y. (2007) Mesoporous silica nanoparticles for drug delivery and biosensing applications. *Adv. Funct. Mater. 17*, 1225–1236.

(10) Trewyn, B. G., Giri, S., Slowing, I., and Lin, V. S.-Y. (2007) Mesoporous silica nanoparticle based controlled release, drug delivery, and biosensor systems. *Chem. Commun.* 3236–3245.

(11) Vallet-Regi, M., Balas, F., and Arcos, D. (2007) Mesoporous materials for drug delivery. *Angew. Chem., Int. Ed. 46*, 7548–7558.

(12) Slowing, I. I., Vivero-Escoto, J. L., Wu, C.-W., and Lin, V. S.-Y. (2008) Mesoporous silica nanoparticles as controlled release drug delivery and gene transfection carriers. *Adv. Drug Delivery Rev. 60*, 1278–1288.

(13) Daniel, M. C., and Astruc, D. (2004) Gold nanoparticles: assembly, supramolecular chemistry, quantum-size-related properties, and applications toward biology, catalysis, and nanotechnology. *Chem. Rev. 104*, 293–346.

(14) Cushing, B. L., Kolesnichenko, V. L., and O'Connor, C. J. (2004) Recent advances in the liquid-phase syntheses of inorganic nanoparticles. *Chem. Rev. 104*, 3893–3946.

(15) Shenhar, R., Norsten, T. B., and Rotello, V. M. (2005) Polymer-mediated nanoparticle assembly: structural control and applications. *Adv. Mater. 17*, 657–669.

(16) Kumar, S., and Nann, T. (2006) Shape control of II-VI semiconductor nanomaterials. *Small 2*, 316–329.

(17) Naik, S. P., Elangovan, S. P., Okubo, T., and Sokolov, I. (2007) Morphology control of mesoporous silica particles. *J. Phys. Chem. C 111*, 11168–11173.

(18) Jurez, B. H., Klinke, C., Kornowski, A., and Weller, H. (2007) Quantum dot attachment and morphology control by carbon nanotubes. *Nano Lett. 7*, 3564–3568.

(19) Wang, Z., and Stein, A. (2008) Morphology control of carbon, silica and carbon/silica nanocomposites: from 3-D ordered macro-/mesoporous monoliths to shaped mesoporous particles. *Chem. Mater. 20*, 1029–1040.

(20) Derfus, A. M., Chan, W. C.-W., and Bhatia, S. N. (2004) Probing the cytotoxicity of semiconductor quantum dots. *Nano Lett. 4*, 11–18.

(21) Sayes, C. M., Gobin, A. M., Ausman, K. D., Mendez, J., West, J. L., and Colvin, V. L. (2005) Nano-C_{60} cytotoxicity is due to lipid peroxidation. *Biomaterials 26*, 7587–7595.

(22) Rozenzhak, S. M., Kadakia, M. P., Caserta, T. M., Westbrook, T. R., Stone, M. O., and Naik, R. R. (2005) Cellular internalization and targeting of semiconductor quantum dots. *Chem. Commun. 17*, 2217–2219.

(23) Kirchner, C., Liedl, T., Kudera, S., Pellegrino, T., Muñoz Javier, A., Gaub, H. E., Stölzle, S., Fertig, N., and Parak, W. J. (2005) Cytotoxicity of colloidal CdSe and CdSe/ZnS nanoparticles. *Nano Lett. 5*, 331–338.

(24) Connor, E. E., Mwamuka, J., Gole, A., Murphy, C. J., and Wyatt, M. D. (2005) Gold nanoparticles are taken up by human cells but do not cause acute cytotoxicity. *Small 1*, 325–327.

(25) Yamawaki, H., and Iwai, N. (2006) Cytotoxicity of water soluble fullerene in vascular endothelial cells. *Am. J. Physiol. Cell Physiol. 290*, C1495–C1502.

(26) Thill, A., Zeyons, O., Spalla, O., Chauvat, F., Rose, J., Auffan, M., and Flank, A. M. (2006) Cytotoxicity of CeO_2 nanoparticles for *Escherichia coli*. Physico-chemical insight of the cytotoxicity mechanism. *Environ. Sci. Technol. 40*, 6151–6156.

(27) Lewinski, N., Colvin, V., and Drezek, R. (2008) Cytotoxicity of nanoparticles. *Small 4*, 26–49.

(28) Wan, Y., Shi, Y., and Zhao, D. (2007) Designed synthesis of mesoporous solids via nonionic-surfactant-templating approach. *Chem. Commun.* 897–926.

(29) Wan, Y., and Zhao, D. (2007) On the controllable soft-templating approach to mesoporous silicates. *Chem. Rev. 107*, 2821–2860.

(30) Wan, Y., Shi, Y., and Zhao, D. (2008) Supramolecular aggregates as templates: ordered mesoporous polymers and carbons. *Chem. Mater. 20*, 932–945.

(31) Lai, C. Y., Trewyn, B. G., Jeftinija, D. M., Jeftinija, K., Xu, S., Jeftinija, S., and Lin, V. S.-Y. (2003) A mesoporous silica nanosphere-based carrier system with chemically removable CdS nanoparticle caps for stimuli-responsive controlled release of neurotransmitters and drug molecules. *J. Am. Chem. Soc. 125*, 4451–4459.

(32) Tang, Q.-L., Xu, Y., Wu, D., Sun, Y.-H., Wang, J., Xu, J., and Deng, F. (2006) Studies on a new carrier of trimethylsilyl-modified mesoporous material for controlled drug delivery. *J. Controlled Release 114*, 41–46.

(33) Vallet-Regi, M. (2006) Ordered mesoporous materials in the context of drug delivery systems and bone tissue engineering. *Chem.—Eur. J. 12*, 5934–5943.

(34) Radu, D. R., Lai, C.-Y., Jeftinija, K., Rowe, E. W., Jeftinija, S., and Lin, V.S.-Y. (2004) A polyamidoamine dendrimers-capped mesoporous silica nanosphere-based gene transfection reagent. *J. Am. Chem. Soc. 126*, 13216–13217.

(35) Giri, S., Trewyn, B. G., Stellmaker, M. P., and Lin, V.S.-Y. (2005) Stimuli-responsive controlled-release delivery system based on mesoporous silica nanorods capped with magnetic nanoparticles. *Angew. Chem., Int. Ed. 44*, 5038–5044.

(36) Slowing, I. I., Trewyn, B. G., and Lin, V. S.-Y. (2006) Effect of surface functionalization of MCM-41-type mesoporous silica nanoparticles on the endocytosis by human cancer cells. *J. Am. Chem. Soc. 128*, 14792–14793.

(37) Slowing, I. I., Trewyn, B. G., and Lin, V. S.-Y. (2007) Mesoporous silica nanoparticles for intracellular delivery of membrane-impermeable proteins. *J. Am. Chem. Soc. 129*, 8845–8849.

(38) Tao, Z., Morrow, M. P., Asefa, T., Sharma, K. K., Duncan, C., Anan, A., Penefsky, H. S., Goodisman, J., and Souid, A. K. (2008) Mesoporous silica nanoparticles inhibit cellular respiration. *Nano Lett. 8*, 1517–1526.

(39) Di Pasqua, A. J., Sharma, K. K., Shi, Y.-L., Toms, B. B., Ouellette, W., Dabrowiak, J. C., and Asefa, T. (2008) Cytotoxicity of mesoporous silica nanomaterials. *J. Inorg. Biochem. 102*, 1416–1423.

(40) Hudson, S. P., Padera, R. F., Langer, R., and Kohane, D. S. (2008) The biocompatibility of mesoporous silicates. *Biomaterials 29*, 4045–4055.

(41) Beyer, R. E. (1967) Preparation, properties and conditions for assay of phosphorylating electron transport particles (ETPH) and its variations. *Methods Enzymol. 10*, 186–194.

(42) Stöber, W., Fink, A., and Bohn, E. (1968) Controlled growth of monodisperse silica spheres in the micron size range. *J. Colloid Interface Sci. 26*, 62–69.

(43) Shi, Y.-L., and Asefa, T. (2007) Tailored core-shell-shell nanostructures: sandwiching gold nanoparticles between silica cores and tunable silica shells. *Langmuir 23*, 9455–9462.

(44) Asefa, T., and Shi, Y.-L. (2008) Corrugated Nanospheres and Nanocages: synthesis via controlled etching and improving chemical delivery and electrochemical and biosensing applications. *J. Mater. Chem. 18*, 5604–5614.

(45) Tao, Z., Penefsky, H. S., Goodisman, J., and Souid, A.-K. (2007) Caspase activation by anticancer drugs: the caspase storm. *Mol. Pharm. 4*, 583–595.

(46) Tao, Z., Jones, E., Goodisman, J., and Souid, A.-K. (2008) Quantitative measure of cytotoxicity of anticancer drugs and other agents. *Anal. Biochem. 381*, 43–52.

TX900276U